Geometric Design for Light Trapping in Bifacial Thin-Film Photovoltaics

Jae-Hyun Kim, Geon-Tae Park, Rira Kang, So-Yeon Ju, Semin Yu, Byunghong Lee, and Sun-Kyung Kim

***Abstract*—Modern photovoltaics (PVs) are increasingly designed to be thinner and more transparent, thus enabling seamless integration into buildings and vehicles in urban environments. However, semitransparent thin-film PVs face inherent challenges in sunlight capture due to the limited volume of absorbing materials and the absence of efficient light-trapping strategies. Herein, we report a geometric design for light trapping in thin-film PVs using a wedge-shaped microprism sheet. This microprism sheet, attached to the planar surface of thin-film PVs, mitigates reflection losses at both external (air-cover) and internal (cover-PV cell) boundaries by leveraging light trapping. The light-trapping effect is quantitatively validated through angle-resolved transmittance measurements. The microprism sheet achieves near-unity external transmittance at all incident angles and redirects 81% of the internally reflected light back to the PV cell over typical solar incidence angles. Outdoor experiments conducted with semitransparent thin-film perovskite (PVSK) PVs demonstrate energy generation enhancements of >17% during daytime in vertically oriented bifacial configurations. These improvements are ascribed to the effective capture of direct sunlight on both the front and rear surfaces of the PVSK PVs. The geometric design of microprism sheets is facile yet effective for broadband light manipulation, offering a versatile solution for advancing solar energy devices and radiative coolers.**

***Index Terms*—Building-integrated photovoltaic, geometric optics, light trapping, microprism, omnidirectional antireflection, upright solar panels.**

I. Introduction

THE mitigation of climate change calls for a significant reduction in greenhouse gas emissions, which, in turn, requires advancements in both energy-generation and energy-saving technologies. The former includes enhancing the efficiency of photovoltaics (PVs) (also frequently referred to as solar cells), thermophotovoltaics, and thermoelectric generators [1], [2], [3], [4], [5], [6], while the latter focuses on the development of passive cooling strategies, such as radiative coolers and energy-saving windows [7], [8], [9], [10], [11], [12], [13], [14], [15], [16], [17], [18], [19].

In recent years, the development of PV technology has shifted toward thinner and more transparent structures, as exemplified by copper indium gallium selenide- [20], [21], [22], perovskite (PVSK)- [23], [24], [25], organic- [26], [27], [28], and amorphous silicon (a-Si)- [29], [30], [31] based PVs, all of which facilitate thin-film processing. Semitransparent thin-film PVs have garnered remarkable attention for their integration into urban infrastructures, particularly in buildings and vehicles, where they can be seamlessly incorporated into window glass and other surfaces requiring visible transparency [32], [33], [34]. In addition, unlike conventional bulk PVs that harness solely sunlight, semitransparent thin-film PVs can generate electricity from both outdoor sunlight and indoor artificial lighting, allowing them to continue generating electricity even after sunset. This bifacial response addresses the availability of PV installation space in densely populated urban environments.

However, the reduced absorber volume in thin-film PVs inherently lowers their external quantum efficiency due to insufficient sunlight capture. Furthermore, integrating traditional antireflective (AR) structures, such as moth-eye patterns, directly into the PV cell surface is nontrivial due to the limited thickness of thin-film PVs (typically <1 μm) [35], [36]. To overcome these challenges, the development of scalable, cost-effective, and efficient light-harvesting strategies tailored specifically for thin-film PV is essential.

Arrays of microstructures or microprism sheets have been investigated for various applications, including three-dimensional displays that enable selective light transmission based on viewing angle [37], AR covers for bulk PVs [38], [39], [40], and cooling films that enhance thermal emission toward the sky while blocking thermal radiation from the ground [41], [42], [43]. Building on their advantages in light management, this study presents a large-area ($>15 \times 15$ cm^2) polyethylene terephthalate (PET)-based microprism sheet tailored to enhance light trapping in vertically oriented thin-film PVs. Our microprism sheets, designed based on the principles of geometric optics, were attached to the planar surface of thin-film PVs. The microprism sheet mitigates reflection losses at both external (air-cover) and internal (cover-PV cell) boundaries by leveraging its light-trapping effect [43], [44], [45]. To quantify the light-trapping effect, we conducted angle-resolved transmittance measurements. In addition, to validate the practical effectiveness of our microprism

Received 27 February 2025; revised 9 April 2025; accepted 22 April 2025. Date of publication 25 April 2025; date of current version 20 May 2025. This work was supported in part by the Hyundai-NGV Program under Grant R232604.0003 and in part by the National Research Foundation of Korea through the Basic Science Research Program under Grant RS-2023-00207966. *(Jae-Hyun Kim, Geon-Tae Park, and Rira Kang contributed equally to this work.) (Corresponding authors: Byunghong Lee; Sun-Kyung Kim.)*

Jae-Hyun Kim, Geon-Tae Park, and Sun-Kyung Kim are with the Department of Applied Physics, Kyung Hee University, Yongin-si 17104, South Korea (e-mail: lucio0217@khu.ac.kr; iharry01@khu.ac.kr; sunkim@khu.ac.kr).

Rira Kang, So-Yeon Ju, and Byunghong Lee are with the Electronic Devices Research Team, Hyundai Motor Group, Uiwang-si 16082, South Korea (e-mail: rira@hyundai.com; sy_ju@hyundai.com; redboho@hyundai.com).

Semin Yu is with the PSC development Dept. Product Development Team 1, UniTest, Pyeongtaek-si 17099, South Korea (e-mail: sam@uni-test.com).

Color versions of one or more figures in this article are available at https://doi.org/10.1109/JSTQE.2025.3564549.

Digital Object Identifier 10.1109/JSTQE.2025.3564549

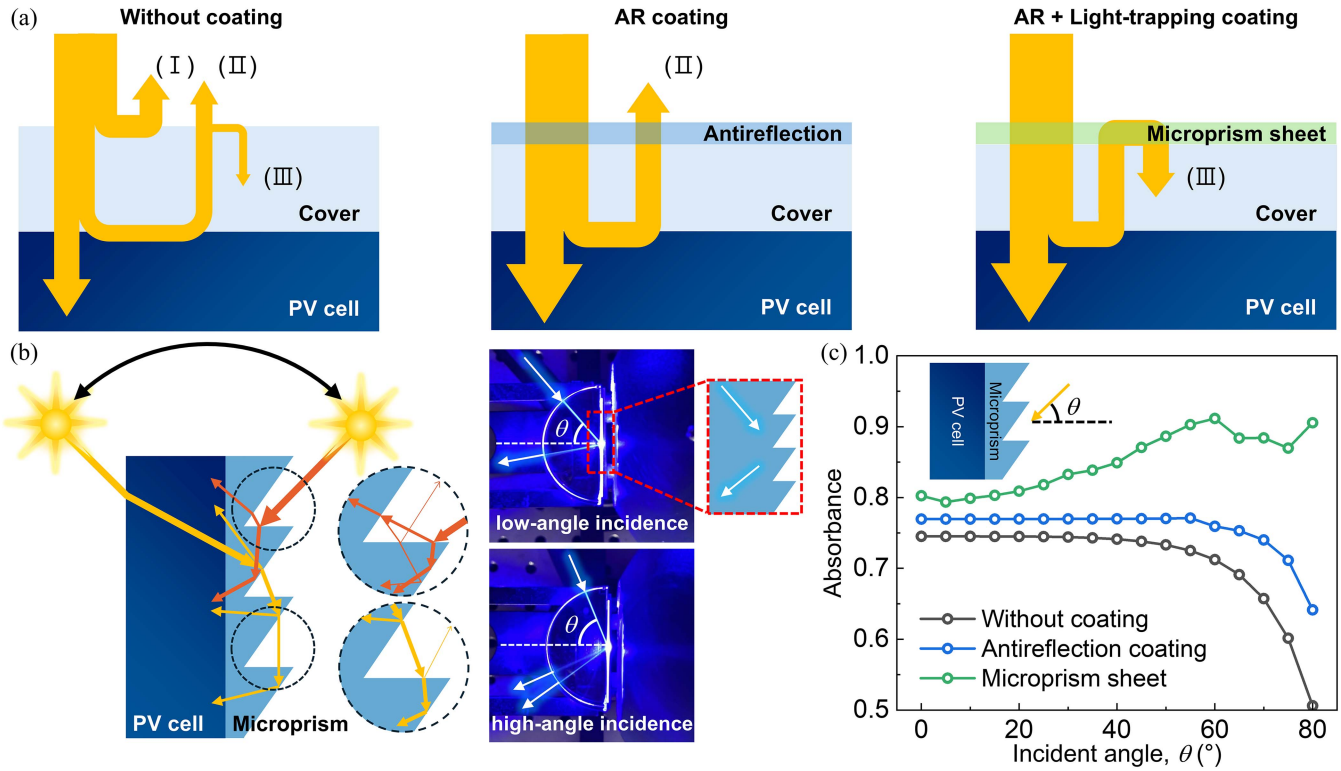

Fig. 1. Conceptual schematics of light-trapping principles. (a) Light pathways in three configurations: uncoated, AR-coated, and a microprism sheet integrating both AR and light-trapping mechanisms. (b) Schematic of a microprism-coated PV cell for front and rear illuminations (left), with photographs showing the light redirection under rear illumination at low and high incidence angles (right). (c) Calculated average (300–1000 nm in wavelength) absorbance of an a-Si PV cell as a function of incident angle for three configurations in (a).

sheet, we performed outdoor experiments using semitransparent thin-film PVSK PVs configured in a vertical orientation.

II. Principles of Light Trapping for Thin-Film PVs

A PV module requires a planar encapsulation cover to protect the PV cell from environmental degradation and mechanical stress [46], [47]. With this encapsulation cover incorporated, strategies for enhancing PV efficiency must address two critical optical effects: reflection losses at the external (air-cover) and the internal (cover-PV cell) boundaries. Fig. 1(a) illustrates three distinct cases: without coating, with an AR coating, and with a light-trapping coating. In the uncoated case, incident light undergoes two primary loss channels: initial reflection at the external boundary (I) and escape of internally reflected light (II). At the internal boundary, light is either reflected at or absorbed into the PV cell, with a portion of reflected light either escaping through the external boundary or being reabsorbed into the PV cell (III). In comparison, the AR coating significantly reduces initial reflection at the air-cover boundary. However, this AR characteristic becomes counterproductive at the cover-cell boundary, making internally reflected light escape into the air (II). To overcome this challenge, our microprism coating is equipped with a light-trapping function. It redirects a major portion of internally reflected light back to the PV cell, thus effectively capturing light that would otherwise be lost after reflection from the internal boundary.

We designed and fabricated a wedge-shaped microprism sheet that combines both AR and light-trapping functions to enhance light absorption in bifacial thin-film PVs (Fig. 1(b)). This design simultaneously minimizes external reflection while redirecting internal reflections back to the PV cell. As illustrated by the yellow (rear incidence) and red (front incidence) rays, the asymmetric microprism morphology enables bifacial sunlight capture, thereby enhancing PV efficiencies under both front and rear illumination conditions. Both front-incidence transmittance and rear-incidence reflectance are driven by multiple refractions and reflections at the horizontal and beveled planes of the microprism. In previous studies, Kim et al. reported an antireflection effect under front-incident illumination of the microprism [38]. For front-incident light, when it first reaches the horizontal plane, a part of the light transmits into the microprism. Even if this transmitted light reaches the beveled plane, total internal reflection occurs at the horizontal plane. The reflected light hits upon the beveled plane and guides into the interior. In contrast, for rear-incident light, when it reaches the beveled plane, some reflect into interior and others transmit. The transmitted light subsequently reaches the horizontal plane, refract, and again reaches the beveled plane. Repeated reflections and refractions along this path ultimately cause most of the light to reflect into the interior. The camera images, taken at low-angle and high-angle incidences using a blue laser under rear illumination, highlight the function of the microprism sheet to redirect incident light toward its origin.

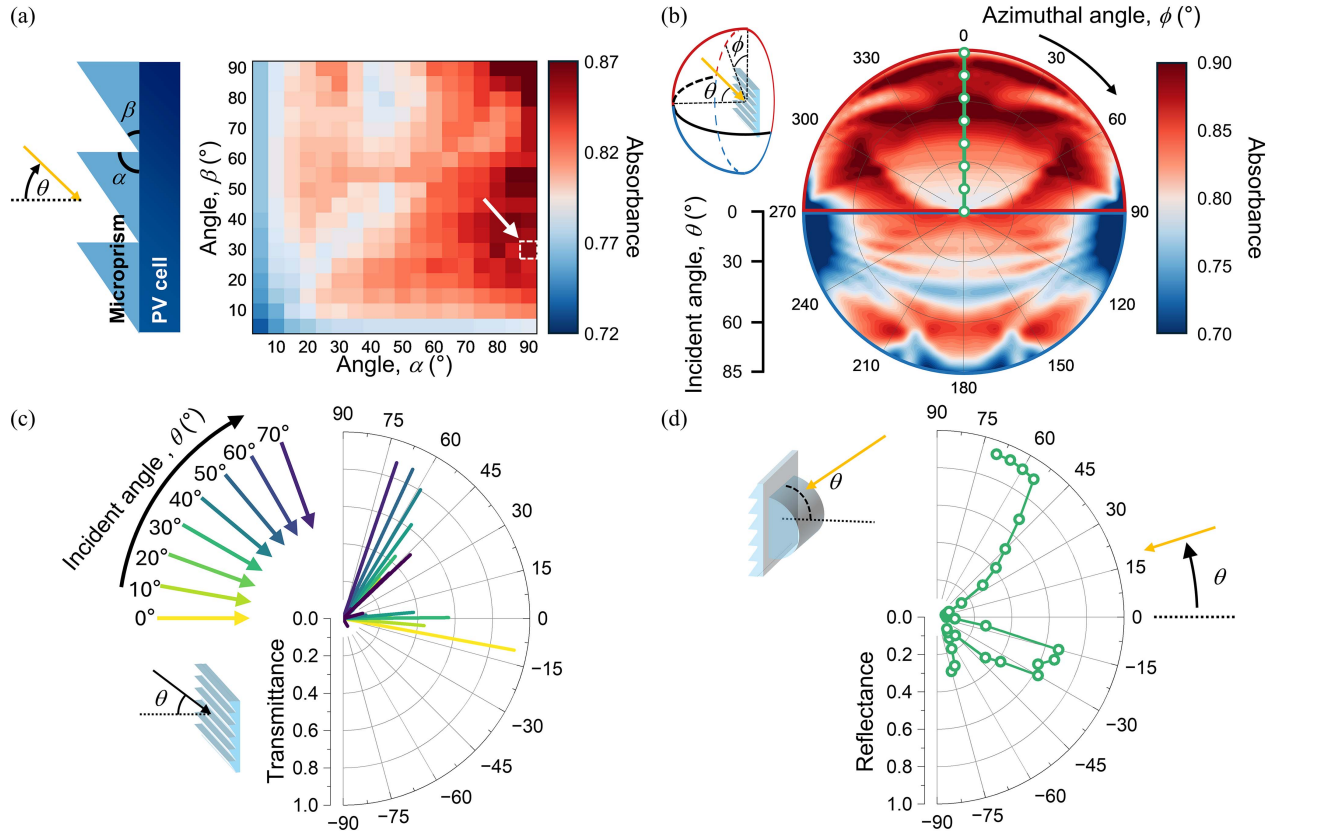

Fig. 2. Quantitative verification of bidirectional light manipulation. (a) Calculated average absorbance of a microprism sheet as functions of base angles α and β, where each data represents absorbance averaged over incident angles (θ) of 0°–85°. The microprism sheet is attached to a semi-infinite a-Si PV cell, as shown in the inset. (b) Calculated absorbance map of the optimized microprism sheet ($\alpha = 90°$ and $\beta = 30°$) plotted as functions of incident (θ) and azimuthal (φ) angles. In the inset, the red region corresponds to light incident from the sky, while the blue region indicates light incident from the ground when the microprism sheet is installed vertically. (c), (d) Measured angular distribution of transmitted light under front illumination with the experimental setup shown in the schematic. (d) Polar plot of reflectance measurements under rear illumination as a function of incident angle.

Fig. 1(c) presents a quantitative comparison of light absorption in a semi-infinite a-Si PV cell across all incident angles. To evaluate the optical performance, we compared three configurations: an uncoated PV cell with a glass cover, a cell with a glass cover coated with an optimized tri-layer AR coating, and a PV cell with our microprism sheet attached to the glass cover. The optimized tri-layer AR coating was designed on a substrate with $n = 1.5$, with each layer (from the substrate side to air) having refractive indices of $n_1 = 1.1067$, $n_2 = 1.2247$, and $n_3 = 1.355$, and thicknesses of $d_1 = 124.2$ nm, $d_2 = 112.3$ nm, and $d_3 = 101.5$ nm, respectively. Among the configurations tested, the uncoated surface exhibits the lowest absorbance due to combined losses from both boundaries (I and II). While the AR coating effectively reduces initial reflection (I), it suffers from the escape of internally reflected light (II). In contrast, our microprism coating achieves the highest overall absorbance by simultaneously suppressing the reflection losses at both interfaces.

III. Bidirectional Light Manipulation

We optimized the cross-sectional morphology of a microprism based on ray-optics simulations to maximize light absorption in a thin-film PV, where we employed a-Si as a PV material (Fig. 2(a)). Fixing the refractive index of microprism medium (1.5) and the pitch of microprism array (250 μm), we focused on the base angles (α and β) of the triangular cross section. While sweeping the entire parameter space of the base angles, we calculated average angular absorbance ($\theta = 0°$–$85°$) in the a-Si cell. The simulation results revealed an optimal geometry with $\alpha \sim 90°$ and $\beta \sim 30°$, yielding approximately 86% absorbance. This optimization accounts for both the AR effect at the external boundary and the rebound effect at the internal boundary, where internally reflected light redirects to the PV cell.

Fig. 2(b) shows the absorbance map of the optimized microprism structure ($\alpha = 90°$ and $\beta = 30°$) as functions of incident angle (θ) and azimuthal angle (φ) under front illumination. The asymmetric microprism geometry maintains a high absorbance of >82% within the upper half of the hemisphere ($-90° < \phi < 90°$), corresponding to the sky-facing region outlined in red. The data extracted at $\phi = 0°$ (green line) corresponds to the simulated result shown in Fig. 1(c). This broadband absorption characteristic indicates the versatility of the microprism design across various installation latitudes and orientations.

To evaluate the light-trapping performance, we experimentally obtained the propagation directions and amplitudes of transmitted and reflected light when the microprism sheet was subject to front (Fig. 2(c)) and rear (Fig. 2(d)) illuminations,

respectively. As shown in Fig. 2(c), the transmitted light splits into two distinct angular lobes. For low-angle incidence (0°–30°), the transmitted light is concentrated within −15°–10°, whereas for high-angle incidence (30°–70°), it is within 50°–70°. Note that the transmittance within the measured $= 0°$ plane for each incident angle can be obtained by integrating the plotted transmittance values over the output angles. The obtained transmittance was approximately 98% for all forward incident angles. This selective angular distribution restricts the transmission angles, which subsequently act as incident angles at the internal boundary, to specific ranges. Notably, in mid-latitude regions such as Seoul, Korea (37.5° N), typical solar incidence angles range between 30° and 70°, thereby precluding the low-angle incidence scenario.

Fig. 2(d) presents the measured reflectance of the microprism sheet under rear illumination through a hemicylindrical prism, which emulates the subsequent reflection of internally reflected light at the cover-air interface. The results show a reflectance exceeding 81% within the 45° to 70° incidence range, closely matching the primary angular lobe (50°–70°) observed under front illumination (Fig. 2(c)). This correspondence results from our optimized design ($\alpha = 90°$, $\beta = 30°$), specifically engineered to align the forward transmission distribution with the angles most effective for internal reflection and trapping. This agreement confirms the light-trapping mechanism; light transmitted through the microprism sheet is deflected to specific angles, then highly reflected at the microprism-air interface, and finally reabsorbed into the PV cell. The integrated effects of AR and light trapping in the optimized microprism design enhance energy harvesting in bifacial thin-film PVs under real-world settings.

IV. Fabrication and Characteristics of Microprism-Coated Thin-Film PVSK PVs

Fig. 3 shows camera images of 15 × 15 cm^2 semitransparent thin-film PVSK PVs used in outdoor experiments, comparing uncoated PVs (Fig. 3(a) and (b)) with microprism-coated PVs (Fig. 3(c) and (d)). The PVSK PVs employed an indium tin oxide (ITO)-based transparent electrode on the front side and an oxide-metal-oxide (OMO) electrode on the rear side. Observation through the cover reveals that while the uncoated PV clearly displays background images (Fig. 3(a)), the microprism-coated PV exhibits significantly reduced transparency (Fig. 3(c)). This optical behavior confirms the rebound effect within the microprism medium, suggesting its potential for applications such as privacy protection, when integrated into buildings or vehicles. From a front viewpoint, the microprism-coated PV exhibits reduced transparency and appears blurred due to multiple refractions and reflections, preventing a clear view of the interior. Notably, observations through the PV cell (Fig. 3(b) and (d)) indicate comparable background visibility in both configurations, validating that the microprism design maintains high transmittance for forward-incident sunlight while preserving bifacial functionality in thin-film PVs. Such a configuration not only maximizes solar absorption on the front side surface but also provides privacy benefits, making it suitable for integration into vertical structures such as buildings and vehicles.

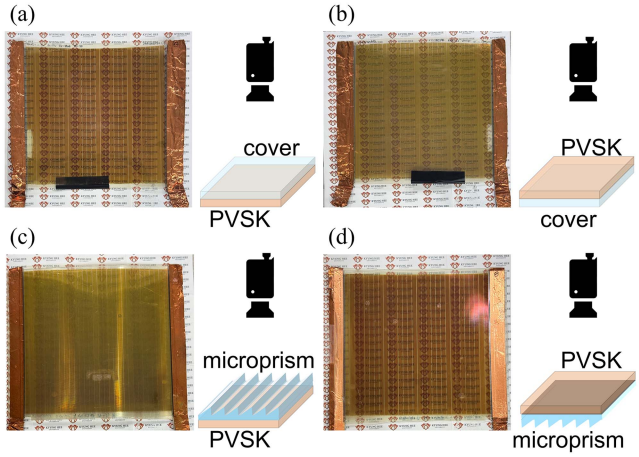

Fig. 3. Camera images of 15 × 15 cm^2 PVSK PVs. Camera images of the uncoated (a), (b) and microprism-coated (c), (d) PVSK PVs captured from the front (a), (c) and rear (b), (d) perspectives. Schematics on the right of each image illustrate the corresponding measurement configurations.

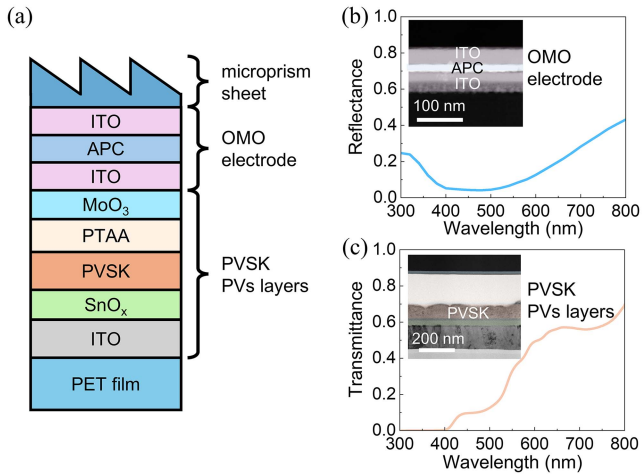

Fig. 4. Structural and optical characterization of microprism-coated PVSK PVs. (a) Schematic of the PET substrate, PVSK PV layers, OMO electrode, and microprism sheet. (b) Measured reflectance spectrum and cross-section TEM image (inset) of the OMO electrode fabricated on a glass substrate. The blue and pink (false-colored) areas indicate APC, and ITO, respectively. (c) Measured transmittance spectrum and cross-section TEM image (inset) of the PVSK PVs layers fabricated on a glass substrate. The brown (false-colored) areas indicate PVSK.

The layer structure of the microprism-coated thin-film PVSK PVs is schematically illustrated in Fig. 4(a). The thin-film PVSK PVs were composed of PET / ITO / SnO_3 (40 nm) / $(FAPbI_3)_x(MAPbBr_3)_{1-x}$ (135 nm) / PTAA (100 nm) / MoO_3 (17 nm) / oxide-metal-oxide (OMO). The OMO electrode, designed for semi-transparency, consisted of an ITO / Ag-Pd-Cu alloy (APC) / ITO stack. The nominal thicknesses of the OMO layers were 35 nm / 14 nm / 35 nm (ITO / APC / ITO), respectively. The OMO electrode was selected for its semi-transparency and flexibility, which are advantageous for bifacial PVs. A wedge-shaped microprism sheet was laminated onto the thin-film PVSK PVs.

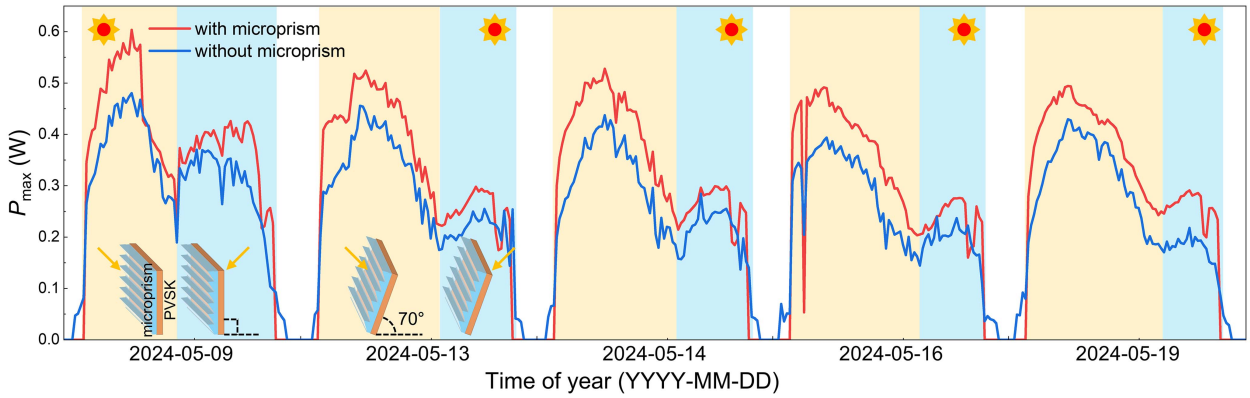

Fig. 5. Maximum power output ($P_{\max}$) of PVSK PVs measured on selected clear days between May 9 and 19, 2024, in Uiwang, Republic of Korea. The PVs were initially installed in a vertical orientation on May 9 and subsequently tilted 20° westward from vertical for the remaining days. Yellow-shaded regions indicate front illumination periods, while blue-shaded regions represent rear illumination periods.

TABLE I
DAILY POWER GENERATION

	May 9		May 13		May 14		May 16		May 19	
	front	rear	front	rear	front	rear	front	rear	front	rear
With microprism total generation (Wh)	2.47	1.95	3.01	1.06	2.99	1.05	2.87	0.87	3.10	0.91
Without microprism total generation (Wh)	2.10	1.65	2.45	0.96	2.32	0.92	2.29	0.75	2.57	0.63
Generation increment (%)	17.46	18.37	22.95	10.45	28.95	13.49	25.12	16.24	20.72	45.52

Comparison of daily power generation between PVs with and without the microprism sheet, separated into sunrise until sunlight reaches the edge of the microprism-coated PV (front) and from that moment to sunset (rear) periods for selected clear days. The power generation increment represents the percentage increase in power output achieved when the microprism sheet is integrated.

All fabrication processes for the thin-film PVSK PVs were carried out in a temperature- and humidity-controlled clean room maintained at 25 °C, 30% RH, and exposed to air. The deposition processes prior to MoO_3 / OMO electrode fabrication were performed by slot-die coating. MoO_3 was thermally evaporated, and OMO (ITO / APC / ITO) was sequentially fabricated in the same sputtering chamber. The microprism sheets were fabricated via roll-to-roll process to enable the production of large-scale microprism-imprinted sheets. First, a uniform, 500-μm-thick layer of urethane acrylate resin was coated onto a PET substrate. Second, a master mold with an inverse pattern of the desired microprism morphology was pressed against the resin-coated PET substrate, transferring the pattern into the resin. Finally, the resin was cured under ultraviolet light to enhance structural robustness. The resulting microprism sheet had a total thickness of 325 μm, consisting of microprism patterns with a height of 145 μm formed on a 180 μm-thick PET substrate film.

A perovskite module with 30 series-connected sub-cells was fabricated on the 15 × 15 cm^2 ITO/PET substrate. The series interconnection of modules was realized through P_1, P_2, and P_3 lines. The lines were patterned using a laser scribing system (Nano-laser) with a wavelength of 355 nm, a frequency of 185 kHz, a power of 1.9 W, and a pulse width of 25 ns. P_1, P_2, and P_3 were scribed before cleaning the ITO / PET substrate, before and after MoO_3 / OMO electrodes. The widths of P_1, P_2, P_3, and dead area were 50, 100, 100 and 410 μm, respectively. The solar cell was encapsulated by moisture barrier films with water vapor transmission rates of 1×10^{-3} g/m^2/day. Finally, a microprism sheets was attached to the encapsulated PVSK PV.

The measured reflectance spectrum of the OMO electrode stack fabricated on a glass substrate is presented in Fig. 4(b), confirming its low visible reflectance beneficial for semi-transparency. The inset cross-sectional transmission electron microscopy (TEM) images revealed that each layer had a controlled thickness, and its interface was sharply discernible. The transmittance spectrum of the PVSK PV layers is shown in Fig. 4(c). The inset TEM image visualizes the cross-section of these active layers.

V. OUTDOOR EXPERIMENTS WITH THIN-FILM PVS

We conducted outdoor experiments in Uiwang, Republic of Korea (37.3° N) from May 9 to 19, 2024, using the PVSK PVs characterized in Fig. 3. The days presented in Fig. 5 and Table I were selected because they were clear days. The average daily temperatures ranged from 13.2 °C to 20.0 °C, and the average cloud cover ranged from 0.1 to 1.4 (i.e., 0 = clear, 10 = overcast) across these measurement days. The PVs were initially installed in a vertical orientation on May 9 and subsequently tilted 20° westward from vertical (corresponding to a 70° angle from the west-side horizontal plane) for the remainder of the

measurements. Fig. 5 illustrates the temporal evolution of maximum power output ($P_{\max}$). The microprism-coated PV, oriented toward the east, experienced two distinct illumination regimes: front illumination from sunrise until sunlight reaches the edge of the microprism-coated PV (yellow-shaded regions) and rear illumination from that moment until sunset (blue-shaded regions). $P_{\max}$ peaked when the solar position optimally aligned with the PV orientation (approximately 9:30). As solar altitude increased, the higher incident angle on the near-vertical PV caused $P_{\max}$ to gradually decline, reaching a local minimum near midday (12:30 on May 9, shifting to 14:00 in subsequent days).

The microprism-coated PV recorded average performance enhancements of 23% under front illumination and 21% under rear illumination compared to the uncoated PV (Table I). The superior front-side enhancement stems from the combined effects of antireflection and light-trapping mechanisms, whereas the rear-side improvement primarily results from light trapping. For practical applications requiring full exposure, the implementation of microprisms on both sides could further optimize light utilization and enhance power generation in bifacial thin-film PVs.

VI. Conclusion

Our geometric-optics approach demonstrates the efficacy of microprism sheets in enhancing both antireflection and light trapping in thin-film PVs. The optimized wedge-shaped design provides consistently high absorbance (>86%) across a broad range of incident angles and wavelengths. Outdoor testing revealed significant power generation improvements enabled by the dual functionality of the microprism sheet: a combination of antireflection and light trapping for front illumination (23% average enhancement), and light trapping for rear illumination (21% average enhancement). These improvements are particularly advantageous for vertical installations in building-integrated PV systems, where the ability to capture oblique and scattered sunlight plays a crucial role in maximizing daily energy yield.

Beyond conventional light management, the versatility of our microprism design allows for various structural adaptations to further enhance performance. For example, double-sided implementation can improve power generation by capturing multidirectional sunlight. Furthermore, the asymmetric triangular geometry enables selective metal coating for added functionality [37], [41], [42]. Specifically, applying a metal layer to the ground-facing surface could suppress downward thermal radiation, thereby enhancing cooling efficiency and extending device longevity. Conversely, a metal coating on the sky-facing surface could facilitate seasonal control of solar radiation, suggesting applications in cooling window technologies. Our current approach, based on PET microprism sheets, inherently exhibits mid-infrared emissivity, suggesting potential radiative cooling effects. By integrating a transparent thermal reflector into this microprism design, it may be possible to achieve directional radiative cooling [43]. These adaptable features highlight how our geometric approach to light manipulation can be extended to address both energy harvesting and thermal management challenges in vertically installed photonic devices.

References

[1] M. L. Brongersma, Y. Cui, and S. Fan, "Light management for photovoltaics using high-index nanostructures," *Nat. Mater.*, vol. 13, no. 5, pp. 451–460, Apr. 2014, doi: 10.1038/nmat3921.

[2] H. A. Atwater and A. Polman, "Plasmonics for improved photovoltaic devices," *Nat. Mater.*, vol. 9, no. 3, pp. 205–213, Feb. 2010, doi: 10.1038/nmat2629.

[3] W. I. Nam, Y. J. Yoo, and Y. M. Song, "Geometrical shape design of nanophotonic surfaces for thin film solar cells," *Opt. Exp.*, vol. 24, no. 14, pp. A1033–A1044, May 2016, doi: 10.1364/OE.24.0A1033.

[4] J.-H. Kim et al., "Synergistically designed antireflective cover for improving wide-angle photovoltaic efficiencies," *Opt. Exp.*, vol. 30, no. 23, pp. 42406–42414, Nov. 2022, doi: 10.1364/OE.476007.

[5] A. LaPotin et al., "Thermophotovoltaic efficiency of 40%," *Nature*, vol. 604, no. 7905, pp. 287–291, Apr. 2022, doi: 10.1038/s41586-022-04473-y.

[6] R. Hu et al., "Machine learning-optimized Tamm emitter for high-performance thermophotovoltaic system with detailed balance analysis," *Nano Energy*, vol. 72, Jun. 2020, Art. no. 104687, doi: 10.1016/j.nanoen.2020.104687.

[7] L. Zhou et al., "A polydimethylsiloxane-coated metal structure for all-day radiative cooling," *Nat. Sustainability*, vol. 2, no. 8, pp. 718–724, Aug. 2019, doi: 10.1038/s41893-019-0348-5.

[8] L. Zhou et al., "Sustainable and inexpensive polydimethylsiloxane sponges for daytime radiative cooling," *Adv. Sci.*, vol. 8, no. 23, Oct. 2021, Art. no. 2102502, doi: 10.1002/advs.202102502.

[9] J.-W. Cho, E.-J. Lee, and S.-K. Kim, "Radiative cooling technologies: A platform for passive heat dissipation," *J. Korean Phys. Soc.*, vol. 81, no. 6, pp. 481–489, Jan. 2022, doi: 10.1007/s40042-022-00402-4.

[10] Y. Zhai et al., "Scalable-manufactured randomized glass-polymer hybrid metamaterial for daytime radiative cooling," *Science*, vol. 355, no. 6329, pp. 1062–1066, Feb. 2017, doi: 10.1126/science.aai7899.

[11] Z. Chen et al., "Can thermal nonreciprocity help radiative cooling?," *Research*, vol. 7, Dec. 2024, Art. no. 0563, doi: 10.34133/research.0563.

[12] S.-B. Seo et al., "Visible transparency modulated cooling windows using pseudorandom dielectric multilayers," *Nanophotonics*, early access, doi: 10.1515/nanoph-2024-0619.

[13] T. Li et al., "A radiative cooling structural material," *Science*, vol. 364, no. 6442, pp. 760–763, May 2019, doi: 10.1126/science.aau9101.

[14] M. Bae, D. H. Kim, S.-K. Kim, and Y. M. Song, "Transparent energy-saving windows based on broadband directional thermal emission," *Nanophotonics*, vol. 13, no. 5, pp. 749–761, Jan. 2024, doi: 10.1515/nanoph-2023-0580.

[15] C. Zhou et al., "3D printed smart windows for adaptive solar modulations," *Adv. Opt. Mater.*, vol. 8, no. 11, Mar. 2020, Art. no. 2000013, doi: 10.1002/adom.202000013.

[16] G. Huang et al., "Radiative cooling and indoor light management enabled by a transparent and self-cleaning polymer-based metamaterial," *Nat. Commun.*, vol. 15, no. 1, May 2024, Art. no. 3798, doi: 10.1038/s41467-024-48150-2.

[17] S. Yu et al., "Ultrahigh visible-transparency, submicrometer, and polymer-free radiative cooling meta-glass coating for building energy saving," *ACS Photon.*, vol. 11, no. 8, pp. 3412–3423, Jul. 2024, doi: 10.1021/acsphotonics.4c00981.

[18] S. Kim et al., "High-performance transparent radiative cooler designed by quantum computing," *ACS Energy Lett.*, vol. 7, no. 12, pp. 4134–4141, Nov. 2022, doi: 10.1021/acsenergylett.2c01969.

[19] G.-T. Park, R. Kang, B. Lee, and S.-K. Kim, "Binary-optimization-based multilayers and their practical applications," *Curr. Opt. Photon.*, vol. 8, no. 6, pp. 545–561, Dec. 2024, doi: 10.3807/COPP.2024.8.6.545.

[20] T. Kato, J.-L. Wu, Y. Hirai, H. Sugimoto, and V. Bermudez, "Record efficiency for thin-film polycrystalline solar cells up to 22.9% achieved by Cs-Treated Cu (In, Ga)(Se, S)$_2$," *IEEE J. Photovolt.*, vol. 9, no. 1, pp. 325–330, Jan. 2019, doi: 10.1109/JPHOTOV.2018.2882206.

[21] Q. Luo et al., "Enhancing photovoltaic performance of perovskite solar cells with silica nanosphere antireflection coatings," *Sol. Energy*, vol. 169, pp. 128–135, Jul. 2018, doi: 10.1016/j.solener.2018.04.044.

[22] M. Nakamura et al., "Cd-free Cu (In, Ga)(Se, S)$_2$ thin-film solar cell with record efficiency of 23.35%," *IEEE J. Photovolt.*, vol. 9, no. 6, pp. 1863–1867, Nov. 2019, doi: 10.1109/JPHOTOV.2019.2937218.

[23] G. Xing et al., "Low-temperature solution-processed wavelength-tunable perovskites for lasing," *Nat. Mater.*, vol. 13, no. 5, pp. 476–480, Mar. 2014, doi: 10.1038/nmat3911.

[24] M. A. Green, A. Ho-Baillie, and H. J. Snaith, "The emergence of perovskite solar cells," *Nat. Photon.*, vol. 8, no. 7, pp. 506–514, Jun. 2014, doi: 10.1038/nphoton.2014.134.
[25] J. Peng et al., "Nanoscale localized contacts for high fill factors in polymer-passivated perovskite solar cells," *Science*, vol. 371, no. 6527, pp. 390–395, Jan. 2021, doi: 10.1126/science.abb8687.
[26] W. Bai et al., "Broadband short-range surface plasmon structures for absorption enhancement in organic photovoltaics," *Opt. Exp.*, vol. 18, no. S4, pp. A620–A630, Oct. 2010, doi: 10.1364/OE.18.00A620.
[27] Q. Gan, F. J. Bartoli, and Z. H. Kafafi, "Plasmonic-enhanced organic photovoltaics: Breaking the 10% efficiency barrier," *Adv. Mater.*, vol. 25, no. 17, pp. 2385–2396, Feb. 2013, doi: 10.1002/adma.201203323.
[28] A. Distler, C. J. Brabec, and H. J. Egelhaaf, "Organic photovoltaic modules with new world record efficiencies," *Prog. Photovolt., Res. Appl.*, vol. 29, no. 1, pp. 24–31, Jan. 2021, doi: 10.1002/pip.3336.
[29] T. Matsui et al., "High-efficiency amorphous silicon solar cells: Impact of deposition rate on metastability," *Appl. Phys. Lett.*, vol. 106, no. 5, Feb. 2015, Art. no. 053901, doi: 10.1063/1.4907001.
[30] H. Sai et al., "Triple-junction thin-film silicon solar cell fabricated on periodically textured substrate with a stabilized efficiency of 13.6%," *Appl. Phys. Lett.*, vol. 106, no. 21, May 2015, Art. no. 213902, doi: 10.1063/1.4921794.
[31] H. Sai, T. Matsui, and K. Matsubara, "Stabilized 14.0% -efficient triple-junction thin-film silicon solar cell," *Appl. Phys. Lett.*, vol. 109, no. 18, Nov. 2016, Art. no. 183506, doi: 10.1063/1.4966996.
[32] J. C. Goldschmidt, "From window to solar cell and back," *Nat. Mater.*, vol. 17, no. 3, pp. 218–219, Jan. 2018, doi: 10.1038/s41563-018-0017-5.
[33] K. Lee et al., "Neutral-colored transparent crystalline silicon photovoltaics," *Joule*, vol. 4, no. 1, pp. 235–246, Jan. 2020, doi: 10.1016/j.joule.2019.11.008.
[34] W. Yu et al., "Highly efficient semitransparent polymer solar cells with color rendering index approaching 100 using one-dimensional photonic crystal," *ACS Appl. Mater. Interfaces*, vol. 7, no. 18, pp. 9920–9928, Apr. 2015, doi: 10.1021/acsami.5b02039.
[35] S. A. Boden and D. M. Bagnall, "Optimization of moth-eye antireflection schemes for silicon solar cells," *Prog. Photovolt.: Res. Appl.*, vol. 18, no. 3, pp. 195–203, Mar. 2010, doi: 10.1002/pip.951.
[36] S. Wilson and M. Hutley, "The optical properties of 'moth eye' antireflection surfaces," *Optica Acta: Int. J. Opt.*, vol. 29, no. 7, pp. 993–1009, Feb. 1982, doi: 10.1080/713820946.
[37] H. Yoon et al., "Arrays of Lucius microprisms for directional allocation of light and autostereoscopic three-dimensional displays," *Nat. Commun.*, vol. 2, no. 1, Aug. 2011, Art. no. 455, doi: 10.1038/ncomms1456.
[38] J.-H. Kim et al., "High-efficiency upright solar panels with antireflective microprism-imprinted sheets," *Cell Reports Phys. Sci.*, vol. 5, no. 4, Apr. 2024, Art. no. 101906, doi: 10.1016/j.xcrp.2024.101906.
[39] S. Jalaly, M. Vahdani, M. Shahabadi, and G. M. M. Sadeghi, "Design, fabrication, and measurement of a polymer-based anti-reflection coating for improved performance of a solar panel under a specific incident angle," *Sol. Energy Mater. Sol. Cells*, vol. 189, pp. 175–180, Jan. 2019, doi: 10.1016/j.solmat.2018.10.001.
[40] Z. Xu, X. Xu, and C. Cui, "Optical functional film with triangular pyramidal texture for crystalline silicon solar cells," *Sol. Energy*, vol. 201, pp. 45–54, May 2020, doi: 10.1016/j.solener.2020.02.081.
[41] J. Zhou et al., "Angle-selective thermal emitter for directional radiative cooling and heating," *Joule*, vol. 7, no. 12, pp. 2830–2844, Dec. 2023, doi: 10.1016/j.joule.2023.10.013.
[42] F. Xie et al., "Subambient daytime radiative cooling of vertical surfaces," *Science*, vol. 386, no. 6723, pp. 788–794, Nov. 2024, doi: 10.1126/science.adn2524.
[43] Q. Cheng et al., "Realizing optimal radiative cooling walls in building-energy nexus via asymmetric emissivity," *Nexus*, vol. 1, no. 3, Sep. 2024, Art. no. 100028, doi: 10.1016/j.ynexs.2024.100028.
[44] J. H. Karp, E. J. Tremblay, and J. E. Ford, "Planar micro-optic solar concentrator," *Opt. Exp.*, vol. 18, no. 2, pp. 1122–1133, Jan. 2010, doi: 10.1364/OE.18.001122.
[45] S. Dottermusch et al., "Micro-cone textures for improved light in-coupling and retroreflection-inspired light trapping at the front surface of solar modules," *Prog. Photovolt., Res. Appl.*, vol. 27, no. 7, pp. 593–602, Jul. 2019, doi: 10.1002/pip.3133.
[46] L. Chen, Q.-K. Wang, P.-H. Wangyang, K. Huang, and X.-Q. Shen, "Light trapping characteristics of glass substrate with hemisphere pit arrays in thin film Si solar cells," *Chin. Phys. B*, vol. 24, no. 4, Apr. 2015, Art. no. 040202, doi: 10.1088/1674-1056/24/4/040202.
[47] M. Kim et al., "Antireflective, self-cleaning and protective film by continuous sputtering of a plasma polymer on inorganic multilayer for perovskite solar cells application," *Sol. Energy Mater. Sol. Cells*, vol. 191, pp. 55–61, Mar. 2019, doi: 10.1016/j.solmat.2018.10.020.
[48] S. Oh et al., "A scalable haze-free antireflective hierarchical surface with self-cleaning capability," *Adv. Sci.*, vol. 9, no. 27, Sep. 2022, Art. no. 2202781, doi: 10.1002/advs.202202781.

Jae-Hyun Kim received the B.S. degree in astronomy and space science and the M.S. degree in physics in 2021 and 2023, respectively from Kyung Hee University, Yongin, Korea, where he is currently working towards the Ph.D. degree in physics. His research interests include anti-reflection, radiative cooling, and energy-saving window technologies based on diffraction, interference, and geometric optics.

Geon-Tae Park received the B.S. degree in applied physics in 2024 from Kyung Hee University, Yongin, Korea, where he is currently working toward the M.S. degree in physics. His research interests include inverse design, multilayer photonic structures, and quantum computing-based machine learning.

Rira Kang received the Ph.D. degree in materials science and engineering from Gwangju Institute of Science and Technology, Gwangju, Korea in 2015. From 2015 to 2017, she was a Postdoctoral Researcher with Korea Atomic Energy Research Institute. She is currently a Senior Research Engineer in Energy Device Research Team with Hyundai Motor Group. Her research focuses on vehicle integrated photovoltaics.

So-Yeon Ju received M.Eng. degree in perovskite solar cells from Inha University, Incheon, Korea in 2023. She is currently a Researcher in the Energy Device Research Team with Hyundai Motor Group. Her research interests include the application of perovskites, especially the development of solar cells for vehicles.

Semin Yu received the B.S. and M.S. degree in chemistry from Hannam University, Daejeon, Korea in 2008 and 2010, respectively. Since 2022, he has been a Senior Researcher with the Perovskite Solar Cells (PSC) development team, UniTest Inc., Gyeonggi-do, Korea. His research focuses on manufacturing processing of perovskite solar cells based on N-I-P structures.

Byunghong Lee received the Ph.D. degree in material science and engineering from Northwestern University, Xi'an, China in 2017. Since 2017, he has been working as a Solar Energy Development Project Leader with Hyundai Motor Group, where he mainly conducts research on energy system development technologies (harvesting, storage, and saving).

Sun-Kyung Kim received the B.S., M.S., and Ph.D. degrees in physics from KAIST in 2000, 2002, and 2006, respectively. From 2006 to 2008, he was a Senior Researcher with LG Electronics. From 2008 to 2010, he was a Chief Researcher with LG Innotek. He was a Postdoctoral Researcher in Chemistry and Chemical Biology at Harvard University from 2010 to 2013. Since 2013, he has been with Kyung Hee University, Yongin, Korea, where he is currently a Tenured Professor in Applied Physics. His research interests include high-index-contrast dielectric or metal/dielectric hybrid photonic materials for manipulating light absorption, light emission, and thermal radiation across the ultraviolet, visible, infrared, and microwave spectra, as well as the realization of optical materials with exceptional dispersion through the concepts of metamaterials and surface plasmons.